IOPscience iopscience.iop.org

Home Search Collections Journals About Contact us My IOPscience

Injectable reactive biocomposites for bone healing in critical-size rabbit calvarial defects

This article has been downloaded from IOPscience. Please scroll down to see the full text article.

2012 Biomed. Mater. 7 024112

(http://iopscience.iop.org/1748-605X/7/2/024112)

View the table of contents for this issue, or go to the journal homepage for more

Download details:
IP Address: 131.84.11.215
The article was downloaded on 04/04/2012 at 18:45

Please note that terms and conditions apply.

Report Documentation Page

Form Approved
OMB No. 0704-0188

Public reporting burden for the collection of information is estimated to average 1 hour per response, including the time for reviewing instructions, searching existing data sources, gathering and maintaining the data needed, and completing and reviewing the collection of information. Send comments regarding this burden estimate or any other aspect of this collection of information, including suggestions for reducing this burden, to Washington Headquarters Services, Directorate for Information Operations and Reports, 1215 Jefferson Davis Highway, Suite 1204, Arlington VA 22202-4302. Respondents should be aware that notwithstanding any other provision of law, no person shall be subject to a penalty for failing to comply with a collection of information if it does not display a currently valid OMB control number.

1. REPORT DATE	2. REPORT TYPE	3. DATES COVERED
29 MAR 2012		**00-00-2012 to 00-00-2012**

4. TITLE AND SUBTITLE	5a. CONTRACT NUMBER
Injectable Reactive Biocomposites For Bone Healing In Critical-Size Rabbit Calvarial Defects	5b. GRANT NUMBER
	5c. PROGRAM ELEMENT NUMBER
6. AUTHOR(S)	5d. PROJECT NUMBER
	5e. TASK NUMBER
	5f. WORK UNIT NUMBER
7. PERFORMING ORGANIZATION NAME(S) AND ADDRESS(ES) **US Army Institute of Surgical Research,3698 Chambers Pass,Fort Sam Houston,TX,78234 ...**	8. PERFORMING ORGANIZATION REPORT NUMBER
9. SPONSORING/MONITORING AGENCY NAME(S) AND ADDRESS(ES)	10. SPONSOR/MONITOR'S ACRONYM(S)
	11. SPONSOR/MONITOR'S REPORT NUMBER(S)

12. DISTRIBUTION/AVAILABILITY STATEMENT
Approved for public release; distribution unlimited

13. SUPPLEMENTARY NOTES
Biomed. Mater. 7 (2012) 024112 (14pp)Published 29 March 2012

14. ABSTRACT

Craniofacial injuries can result from trauma, tumor ablation, or infection and may require multiple surgical revisions. To address the challenges associated with treating craniofacial bone defects, an ideal material should have the ability to fit complex defects (i.e. be conformable), provide temporary protection to the brain until the bone heals, and enhance tissue regeneration with the delivery of biologics. In this study, we evaluated the ability of injectable lysine-derived polyurethane (PUR)/allograft biocomposites to promote bone healing in critical-size rabbit calvarial defects. The biocomposites exhibited favorable injectability, characterized by a low yield stress to initiate flow of the material and a high initial viscosity to minimize the adverse phenomena of extravasation and filter pressing. After injection, the materials cured within 10?12 min to form a tough, elastomeric solid that maintained mechanical integrity during the healing process. When injected into a critical-size calvarial defect in rabbits, the biocomposites supported ingrowth of new bone. The addition of 80 μg mL−1 recombinant human bone morphogenetic protein-2 (rhBMP-2) enhanced new bone formation in the interior of the defect, as well as bridging of the defect with new bone. These observations suggest that injectable reactive PUR/allograft biocomposites are a promising approach for healing calvarial defects by providing both mechanical stability as well as local delivery of rhBMP-2.

15. SUBJECT TERMS

16. SECURITY CLASSIFICATION OF:			17. LIMITATION OF ABSTRACT	18. NUMBER OF PAGES	19a. NAME OF RESPONSIBLE PERSON
a. REPORT	b. ABSTRACT	c. THIS PAGE			
unclassified	**unclassified**	**unclassified**	**Same as Report (SAR)**	**16**	

Biomed. Mater. **7** (2012) 024112 (14pp) doi:10.1088/1748-6041/7/2/024112

Injectable reactive biocomposites for bone healing in critical-size rabbit calvarial defects

Jerald E Dumas[1,2,6,7], Pamela B BrownBaer[3,6], Edna M Prieto[1,2], Teja Guda[3,4], Robert G Hale[3], Joseph C Wenke[3] and Scott A Guelcher[1,2,5,8]

[1] Department of Chemical and Biomolecular Engineering, 2301 Vanderbilt Place, Vanderbilt University, Nashville, TN, USA
[2] Center for Bone Biology, Vanderbilt University Medical Center, Nashville, TN, USA
[3] US Army Institute of Surgical Research, 3698 Chambers Pass, Fort Sam Houston, TX, USA
[4] Department of Biomedical Engineering, University of Texas at San Antonio, San Antonio, TX, USA
[5] Department of Biomedical Engineering, 2301 Vanderbilt Place, Vanderbilt University, Nashville, TN, USA

E-mail: scott.guelcher@vanderbilt.edu

Received 18 August 2011
Accepted for publication 1 February 2012
Published 29 March 2012
Online at stacks.iop.org/BMM/7/024112

Abstract

Craniofacial injuries can result from trauma, tumor ablation, or infection and may require multiple surgical revisions. To address the challenges associated with treating craniofacial bone defects, an ideal material should have the ability to fit complex defects (i.e. be conformable), provide temporary protection to the brain until the bone heals, and enhance tissue regeneration with the delivery of biologics. In this study, we evaluated the ability of injectable lysine-derived polyurethane (PUR)/allograft biocomposites to promote bone healing in critical-size rabbit calvarial defects. The biocomposites exhibited favorable injectability, characterized by a low yield stress to initiate flow of the material and a high initial viscosity to minimize the adverse phenomena of extravasation and filter pressing. After injection, the materials cured within 10–12 min to form a tough, elastomeric solid that maintained mechanical integrity during the healing process. When injected into a critical-size calvarial defect in rabbits, the biocomposites supported ingrowth of new bone. The addition of 80 μg mL^{-1} recombinant human bone morphogenetic protein-2 (rhBMP-2) enhanced new bone formation in the interior of the defect, as well as bridging of the defect with new bone. These observations suggest that injectable reactive PUR/allograft biocomposites are a promising approach for healing calvarial defects by providing both mechanical stability as well as local delivery of rhBMP-2.

(Some figures may appear in colour only in the online journal)

Abbreviations

ACS	absorbable collagen sponge
BC	biocomposite
CPC	calcium phosphate cement
CSD	critical-size defect
DPG	dipropylene glycol
HA	hydroxyapatite
LTI	lysine triisocyanate
NZW	New Zealand White
PEG	poly(ethylene glycol)

[6] Co-first authors.
[7] Currently at Department of Biomedical Engineering, 315 Ferst Street, Georgia Institute of Technology/Emory University, Atlanta, GA, USA.
[8] Author to whom any correspondence should be addressed.

 © 2012 IOP Publishing Ltd Printed in the UK & the USA

PUR	polyurethane
RCP	random close-packing
rhBMP-2	recombinant human bone morphogenetic protein-2
TCP	tricalcium phosphate
TEDA	triethylene diamine
TRAP	tartrate-resistant acid phosphatase
VEGF	vascular endothelial growth factor

Introduction

Craniofacial injuries can result from trauma, tumor ablation, developmental anomalies, and infection, and in the most severe cases may require multiple surgical revisions [1]. The treatment of craniofacial bone defects presents challenges associated with the need to provide protection to the brain while preventing infection and maintaining adequate cosmesis [2]. Craniofacial bones are either flat (skull) or irregularly shaped (face) and typically consist of two tables of cortical bone with a cancellous bone core (the diploe) that provides a minimal supply of osteoblastic precursor cells within the bone [3]. The curvature of craniofacial bones also poses a challenge to restoration of anatomic form.

Due to its osteogenic and osteoconductive properties, autograft bone is the current standard of care to treat craniofacial bone defects. However, limited supply and donor site morbidity limit its use [4], and long-term results in craniofacial reconstruction are unreliable due to bone resorption resulting in loss of volume and contour [5]. Treatment of congenital defects in children between the ages of 2 and 10 is particularly challenging as they have lost the ability to spontaneously heal, and split calvarial grafts [6] are not adequate due to the underdeveloped diploic space [7, 8]. On the battlefield, craniomaxillofacial injuries caused by explosive devices are characterized by open wounds and comminuted fractures, and in severe cases, complicated by avulsion of soft tissue and burns [9, 10].

Currently, several treatments are used clinically for craniofacial reconstruction and augmentation, including cement pastes, osteoactive biomaterials, and prefabricated polymers [5]. Calcium phosphate cements (CPCs, e.g. Norian® CRS hydroxyapatite cement) offer several advantages, such as injectability, high compressive strength, and chemical bonding to bone [11–13]. When injected into critical-size calvarial defects in New Zealand White (NZW) rabbits, Norian® supported a modest amount of new bone formation at 6 and 12 weeks (1.4% and 11.7%, respectively) [13, 14]. However, cellular infiltration into the material after 12 weeks was negligible and only appositional bone formation was observed. Adverse effects on the host soft tissue were observed in some cases due to fragmentation of the cement, which has been attributed to pulsatile forces arising from the dura [15]. Thus, while the compressive strength of CPCs exceeds that of trabecular bone, the shear properties of these materials under physiologically relevant dynamic loads are weak [16]. Non-settable pastes comprising particulated allograft or demineralized bone matrix (DBM) dispersed in a flowable carrier have also been investigated. An injectable DBM/glycerol biocomposite has been reported to heal rabbit calvaria critical-size defects (CSDs) after 12 weeks [2]. However, since the material is non-settable, it has weak mechanical properties and does not provide immediate protection to the brain [14].

Recombinant human bone morphogenetic protein 2 (rhBMP-2), a potent growth factor that plays an important role in the membranous healing of the craniofacial skeleton [17], has been studied for the treatment of CSDs [18–20]. The use of rhBMP-2 delivered on an absorbable collagen sponge (ACS) has been approved by FDA for single-level anterior lumbar interbody fusion and periodontal ridge augmentation (INFUSE® bone graft) [21, 22]. When implanted in a rabbit calvarial CSD, rhBMP-2 delivered on the ACS carrier promoted >95% ossification of the defect as early as five weeks, compared to <35% for the empty defect and ACS carrier alone [20]. However, the applicability of the collagen sponge in craniofacial defects is limited by its weak mechanical properties and consequent inability to provide space maintenance [5, 23, 24].

To address the challenges of craniofacial repair, an ideal material should have the ability to fit complex defects (i.e. be conformable), harden to provide temporary protection until tissue remodels (i.e. be settable), and enhance tissue regeneration with the delivery of biologics [25, 26]. In this study, we evaluated the ability of injectable lysine-derived polyurethane (PUR)/allograft biocomposites (BCs) to promote bone healing in critical-size rabbit calvarial defects. The biocomposites have initial compressive strength comparable to that of trabecular bone and support cellular infiltration and bone remodeling in femoral plug defects in rats [27] and rabbits [28]. In the present study, the potential of injectable biocomposites incorporating 18 vol% allograft bone particles, 35 vol% polymer, and 47% pores to enhance bone healing in 15 mm calvarial defects in rabbits was investigated. The efficacy of the biocomposites as an injectable delivery system for rhBMP-2 to enhance new bone formation was also evaluated.

Materials and methods

Materials

LTI-PEG prepolymer (21.7% NCO) and polyester triol (900 g mol^{-1}) were obtained from Ricerca Biosciences (Concord, OH). The backbone of the polyester triol comprised 60% caprolactone, 30% glycolide, and 10% lactide. The gelling catalyst triethylene diamine (TEDA) and dipropylene glycol (DPG) were purchased from Sigma-Aldrich (St. Louis, MO). An Infuse® Bone graft kit was acquired from Medtronic (Minneapolis, MN). Rabbit allograft mineralized bone particles (sieved to 105–500 μm) were provided by Osteotech, Inc. (Eatontown, NJ). Norian® CRS, a hydroxyapatite-based CPC, was purchased from Synthes, Inc. (West Chester, PA).

Preparation of rhBMP-2

A solution of rhBMP-2 (1.5 mg mL^{-1}) was prepared by reconstituting rhBMP-2 powder per mixing instructions

provided with the Infuse kit. The solution was aliquoted into vials to achieve 80 μg mL^{-1} of active rhBMP-2 dose in each sample. The vials were frozen at −80° C and lyophilized to achieve a powder.

Synthesis of the injectable biocomposite

An index of 125 was targeted to produce a biocomposite with a porosity of 47% upon injection as described previously [27]. The TEDA catalyst was blended with DPG to yield a 10% solution of TEDA. Hydroxyl equivalents from the polyester triol, the DPG carrier, and water were included in the index calculation:

$$\text{INDEX} = 100 \times \frac{\text{NCO Eq}}{\text{OH Eq (Triol)} + \text{OH Eq (Water)} + \text{OH Eq (DPG)}}. \quad (1)$$

The appropriate amounts of polyester triol, LTI-PEG prepolymer, and allograft bone particles (180 μm) were added to a mixing cup and mixed for 90 s. The allograft loading was 45 wt% of the resulting paste, which was then added to the rhBMP-2 vial followed by the addition of TEDA. After mixing for 60 s, the biocomposite (BC) was poured in between parallel plates for rheological characterization, or injected into either molds for mechanical testing or into rabbit calvarial defects.

Rheological properties

In order to characterize the injectability of the biocomposites, the rheological properties of non-setting samples were determined using a TA Instruments AR-2000ex rheometer. Samples ($n = 3$) were prepared without catalyst, poured between two 25 mm diameter parallel plates, and compressed to a gap of 1000 μm. The material was allowed to flow between the plates to cover the whole area and excess material was removed. The samples were then subjected to a dynamic frequency sweep (0.1 to 100 rad s^{-1}) at 25 °C with controlled strain amplitude of 0.02%. A Cox Merz transformation was applied to the dynamic data to obtain the steady state viscosity (η, Pa*s) and shear stress (τ, Pa) as a function of shear rate (γ, s^{-1}). The shear stress (τ) versus shear strain (γ) data were fit to the Casson model by plotting $\tau^{1/2}$ versus $\gamma^{1/2}$ at low strains [29] and extrapolated to zero shear rate to estimate the yield stress (τ_{CA}) [29, 30]:

$$\sqrt{\tau} = \sqrt{\tau}_{CA} + \sqrt{\eta_{CA}}\sqrt{\gamma} \quad (2)$$

where η_{CA} is the Casson plastic viscosity.

Mechanical properties

Cylindrical specimens (6 mm diameter × 12 mm long) of biocomposites with and without rhBMP-2 were prepared by injecting the materials into a plastic mold. Samples ($n = 4$) were hydrated for 24 h in PBS and then tested for compression using an MTS 898 equipped with a 13 kN load cell. The samples were preloaded to 12 N, followed by compression at a constant strain rate of 6 mm min^{-1} until failure. Load and displacement were recorded and transformed to stress and strain using the initial sample cross-sectional area and height respectively. The stress–strain curve was used to determine the Young's modulus, compressive strength (maximum stress), yield stress and strain, and energy-to-failure (area under the curve calculated at the yield point) of the samples.

Table (*A*)	Empty Defect (negative control)	CPC (clinical control)	BC	BC + rhBMP-2
6 weeks	10	10	10	10
12 weeks	10	10	10	-

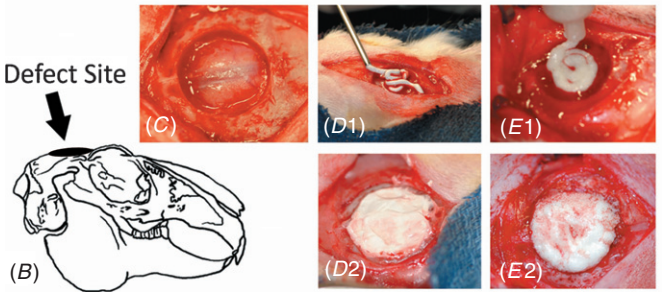

Figure 1. Design of the NZW rabbit calvarial CSD study. (*A*) Table listing the study design. (*B*) Illustration of the rabbit calvarium showing the location of the defect. (*C*) Photograph of the empty defect. (*D*) Photographs of the CPC during injection (*D*1) and cure (*D*2). (*E*) Photographs of the biocomposite during injection (*E*1) and cure (*E*2).

Rabbit study

Animal experiments were been conducted in compliance with the Animal Welfare Act, the implementing Animal Welfare Regulations, and the principles of the Guide for the Care and Use of Laboratory Animals. As shown in figure 1, four treatment groups were evaluated in this animal study using skeletally mature New Zealand White rabbits at two time points, 6 and 12 weeks. An empty defect was included as the negative control, and the injectable calcium phosphate cement (CPC) was used as the clinical control. The effects of rhBMP-2 delivered from the biocomposite were also investigated at six weeks. Considering a recent study reporting that addition of rhBMP-2 to CPC (Norian) did not significantly enhance remodeling of the cement in a rat calvarial defect model [31], the CPC + rhBMP-2 group was not included in the study design. Furthermore, CPCs loaded with rhBMP-2 are not approved for clinical use and are thus not typically used in the clinic. Following standard practices for aseptic surgery, a full-thickness calvarial defect was prepared in the parietal bones using a 15 mm surgical trephine for rabbits as described previously (figure 1(*B*)) [32]. Briefly, upon the surgical exposure of the cranium, a MicroAire surgical handpiece with a brass trephine was used to create the critical-size defect (CSD) of 15 mm during copious saline irrigation (figure 1(*C*)). The cranial cap was carefully removed to separate the attached dura from the underside of the cap. Pressure with sterile gauze was applied to stop bleeding. The defects were treated by injection of the CPC (figure 1(*D*)) or biocomposite (figure 1(*E*)) according to the pre-determined randomization scheme. Soft tissues were closed in layers using resorbable

3–0 Dexon sutures to create two sets of continuous sutures. The animals were euthanized at the given endpoints.

Radiographic analysis

Radiographs were acquired using a Faxitron MX20 x-ray Digital System (Faxitron x-ray Corporation, Wheeling, IL) for each calvarium after extraction. The images were captured at 25 kV at a 15 s exposure time and imported into the Faxitron DR Software (Version 3.2.2). For quantification, the images were exported as a BITMAP file using window levels 1396/184. CTAn software v1.11 (Skyscan, Kontich, Belgium) was used to analyze the% defect area coverage and relative x-ray attenuation through the defect thickness for each treatment group. A region identical to the size of the defect created during the original study was outlined on each x-ray, and automated thresholding was performed within this region using the Otsu method [33] across all samples to determine the mineralized tissue within the defect. The percent of the defect area filled by the mineralized tissue was measured as a ratio of the pixels of gray above the threshold to the total number of pixels in the defect area. The relative x-ray attenuation through the defect was determined as the ratio of the mean grayscale level of the mineralized tissue within the defect to the mean grayscale value of the mineralized tissue of the surrounding host bone.

Histology and histomorphometry

The calvaria were placed in a solution of 10% neutral buffered formalin followed by a series of ethanol dehydrations. The specimens were then embedded in methyl/butyl methacrylate. The resulting blocks were then sectioned using an Exakt system, producing 75 μm sections that were stained with Sanderson's rapid bone stain counterstained with van Gieson. The advantage of this stain is that residual allograft bone can be distinguished from new bone under higher magnification [28]. Bone was stained red with osteocytes, osteoblasts and osteoclasts stained dark blue, residual polymer stained black, red blood cells stained turquoise and other cells stained a lighter blue. Quantifying the residual material (CPC or polymer), allograft bone, and new bone formation required the use of high magnification. Therefore, three zones progressing from the edge of the defect to the center region were examined at 40X magnification with and without polarizing the light. The edge of the defect was determined by visualizing (at 40X magnification) and then marking the disruption of the linear pattern of the calvarial bone and cells resulting from the surgical creation of the defect. To differentiate between the new bone and the residual allograft the allograft bone was quantified in these zones by meeting the following three criteria: (1) acellular, (2) angular in shape, and (3) illuminated under polarized light. In addition, the total amount of bone in the defect area was quantified using a stitched image taken with an Olympus camera (DP71) at 10X magnification (Microscope Olympus SZX16). Adobe Photoshop (CS3) was utilized to stitch the images together and to complete the histomorphometry (Version 7.0.1). Histomorphometry data were obtained by using color thresholding and an image layering technique to quantify the pixels of each layer and compare it to the total pixels in the area of interest. Additional sections were stained for tartrate-resistant acid phosphatase (TRAP) expressed by osteoclasts. Thin (5 μm) sections were deplasticized, rehydrated, stained for TRAP, and counterstained with hematoxylin. Images were obtained at 20X magnification and osteoclasts were identified as multinucleated red cells.

Table 1. Mechanical properties of the biocomposite (BC) and Norian CRS measured under compressive loads (value ± standard error of the mean).

	Compression	
Property	BC	Norian
Young's modulus (MPa)	53.2 ± 12.1	796.1 ± 307.0
Yield stress (MPa)	4.06 ± 0.03	8.53 ± 3.83
Yield strain (%)	11.4 ± 2.3	1.3 ± 0.2
Compressive strength (MPa)	N/A	15.9 ± 3.4
Energy-to-failure (kJ m^{-3})	3122 ± 404[a]	297 ± 121[b]

[a] Measured up to 50% strain.
[b] Measured up to peak.

Results

Injectability of biocomposites

The working time of the biocomposite, as measured as the time after which the material could not be injected from the syringe, was 4.5 min [27]. The tack-free time, corresponding to the time when the material did not stick to a metal spatula, was 12 min. Solid-filled suspensions typically exhibit a yield stress, which is the pressure that must be applied to initiate flow of the material [29]. To characterize the injectability of the biocomposites, both the yield stress required to initiate flow of the material (τ_{CA}) as well as the viscosity η were measured for the non-setting form of the composite [30]. The values of τ_{CA} and η_{CA} determined from the shear stress versus shear rate plot (figure 2(*A*)) fit to the Casson model were 2.1 Pa and 199 Pa*s, respectively. The viscosity data (figure 2(*B*)) show that the biocomposite is shear-thinning (i.e. the viscosity decreases with increasing stress), and the viscosity at 5 s^{-1} (the recommended shear rate at which viscosity should be reported [30]) is 170 Pa*s. The combination of a low yield stress and shear-thinning behavior is desirable, since after initial application of a relatively small force the material flows readily into the defect, and subsequently stops flowing after the removal of the force.

Compression properties of the CPC and biocomposite

The porosity was 47 vol% and the pore size was 177 ± 90 μm, resulting in an allograft fraction of 17.5 vol% [27]. Representative stress–strain curves for the biocomposite and CPC measured under compression are shown in figure 3. As listed in table 1, the CPC failed due to brittle fracture at 1.0 ± 0.2% strain and exhibited compressive strength of 15.9 ± 3.4 MPa. In contrast, the biocomposite exhibited plastic behavior and did not fracture at strains up to 50%

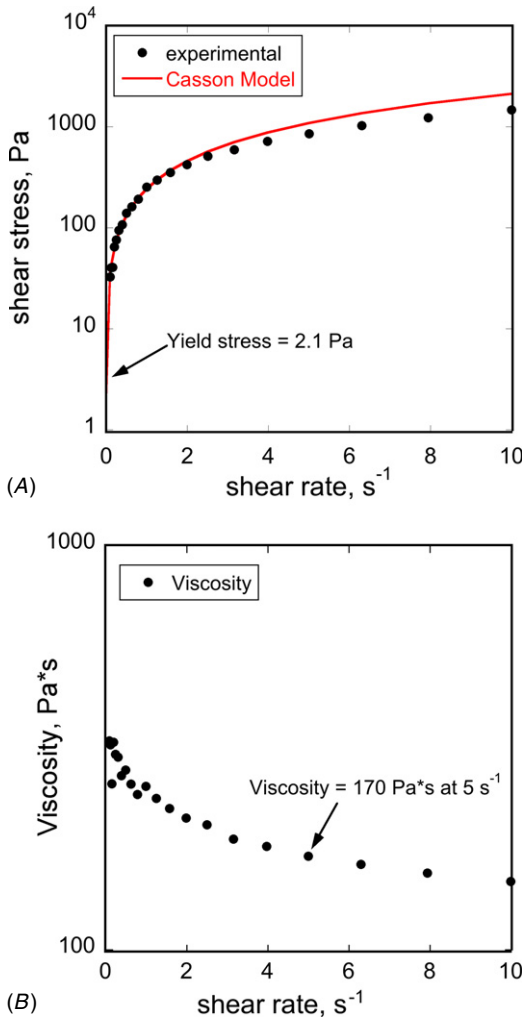

Figure 2. Rheological data measured for the non-setting form of the biocomposite to characterize the injectability. (*A*) Shear stress versus shear rate. Data were fitted to the Casson model (solid line) used to predict the rheological properties of solid-filled suspensions and to calculate the yield stress (arrow). (*B*) Viscosity versus shear rate.

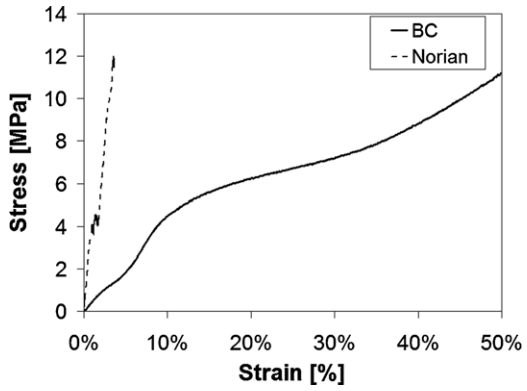

Figure 3. Representative stress–strain curves for the biocomposite and CPC measured under compressive loads. The area under the curve represents the energy-to-failure of the material.

[27]. The yield strength of the biocomposite was 4.06 ± 0.03 MPa, above which the material continued to undergo plastic deformation up to 11.4 ± 2.3% strain [27]. The energy-to-failure, which is approximated by the area under the stress–strain curve, was 297 ± 121 kJ m^{-3} for the CPC and 3122 ± 404 kJ m^{-3} for the biocomposite. Incorporation of rhBMP-2 in the biocomposites did not have a significant effect on mechanical properties (data not shown).

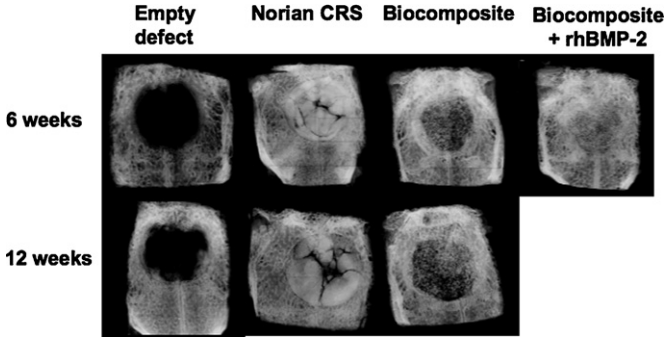

Figure 4. Representative radiographs of the empty defect, CPC, biocomposite, and biocomposite + rhBMP-2 at 6 and 12 weeks.

Injection of the CPC and biocomposites in calvarial defects

During the surgical procedure, no treatment, the CPC or one of the biocomposite groups was injected in the defect, which had a volume of approximately 0.5 mL (figure 1(*C*)). A total of 0.25 mL of the biocomposite was used to fill the defect as it expanded in volume during cure (figure 1(*E*)). After cure, both the CPC and biocomposite showed good contact with host bone (figure 1(*D* and *E*)). Some of the defects treated with the CPC developed cracks immediately after cure, which were observed before closure of the wound, while no cracks were observed for the biocomposites.

Radiographic analysis

Radiographs (figure 4) of the negative control defects showed minimal bone formation near the edges of the defect at both 6 and 12 weeks, as anticipated for a CSD. Consistent with observations during surgery, x-rays of the CPC treatment group showed cracking of the material. Bone ingrowth was observed around the perimeter of the biocomposite treatment groups with traces of bone in the center. X-ray images of the BC + rhBMP-2 group suggested a substantial increase in new bone formation within the defect relative to the other treatment groups.

In figure 5(*A*), the relative density (as approximated by the radio-opacity of the defect relative to the host bone) calculated using the CTAn software is plotted for each treatment group. The relative density was calculated for all groups by normalizing the attenuation of the defect region by the attenuation observed in the calvarial bone (approximately equal in area to the defect) around the defect site. The attenuation of allograft or regenerating bone asymptotically approaches that of the host calvarial bone, implying that the relative density approaches 100% [34]. In contrast, the attenuation of pure hydroxyapatite is significantly greater than that of native bone, and as the mineral resorbs and is replaced by new bone, the attenuation decreases and asymptotically approaches that of host bone. Thus, while the CPC showed significantly higher (>100% of the density of host bone)

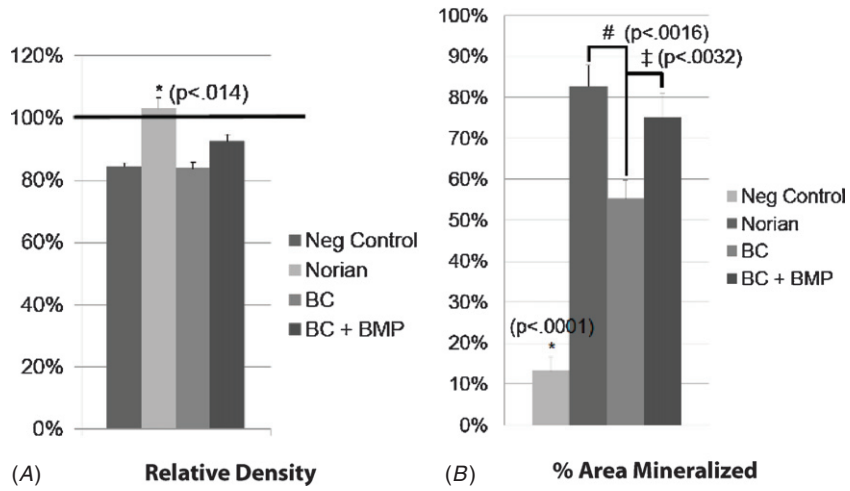

Figure 5. Quantitative analysis new bone formation by analysis of radiographs for each treatment group at six weeks. (*A*) Relative density of the defect compared to the host bone. (*B*) Percentage area mineralized material in the defect.

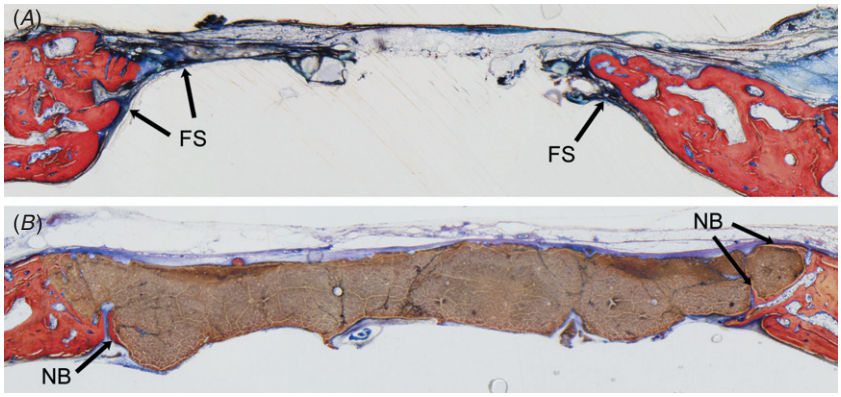

Figure 6. Representative histological sections of (*A*) an empty defect and (*B*) a CPC-treated defect. New bone formation (denoted by NB, highlighted by arrows) was observed near the edges of the defect. FS denotes dense connective tissue consistent with fibrotic scarring.

relative density ($p < 0.02$) compared to the other treatment groups at six weeks, the majority of the mineral content measured derived from residual hydroxyapatite and not new bone formation. There were no significant differences in relative density between the biocomposite treatment groups ($p = 0.08$). Figure 5(*B*) shows the area% mineralization (as approximated by the percentage of the defect filled with tissue having density comparable to that of the host bone) for each treatment group. As expected, there was significantly less mineralized tissue in the negative control compared to the other treatment groups ($p < 0.0001$). In addition, the percent defect area covered was significantly greater in the CPC and BC + rhBMP-2 groups compared to the BC only group ($p < 0.05$). However, since CTAn analysis cannot differentiate between calcium phosphate, allograft, or new bone within the mineralized tissue, differences between the CPC and BC + rhBMP-2 groups were not significant.

Histology and histomorphometry

Histological sections indicate that there were no adverse responses to any of the treatment groups used in this study. As expected, a fibrous scar filled the untreated defect at both time points (figure 6(*A*)). The CPC treatment groups (figure 6(*B*)) showed appositional bone growth around the surface and between the cracks of the material as evidenced by the mineralization stained in pink. However, there was no cellular infiltration into the cement. This pattern was the same for both the 6 and 12 week CPC groups, and confirms that the majority of mineral content measured by the radiographic analysis for the CPC group is derived from residual hydroxyapatite and not new bone formation. Figure 7(*A–C*) shows a representative histological section of a biocomposite sample at the six week time point, at which time cells (stained light blue) had infiltrated throughout the volume of the material. Near the host bone/biocomposite interface, new bone lined with osteoid (stained light green) formed within the pores of the material. There was a moderate amount of residual polymer (stained black) remaining within the biocomposite. Representative histological sections at 12 weeks for the biocomposite treatment group (figure 7(*D–F*)) showed extensive polymer degradation as well as new bone formation.

Representative histological sections of the BC + rhBMP-2 treatment group (figure 8) revealed extensive bone growth around the composite as well as throughout the pores of the material. While the cellular density of the core region in the center of the histological section shown in

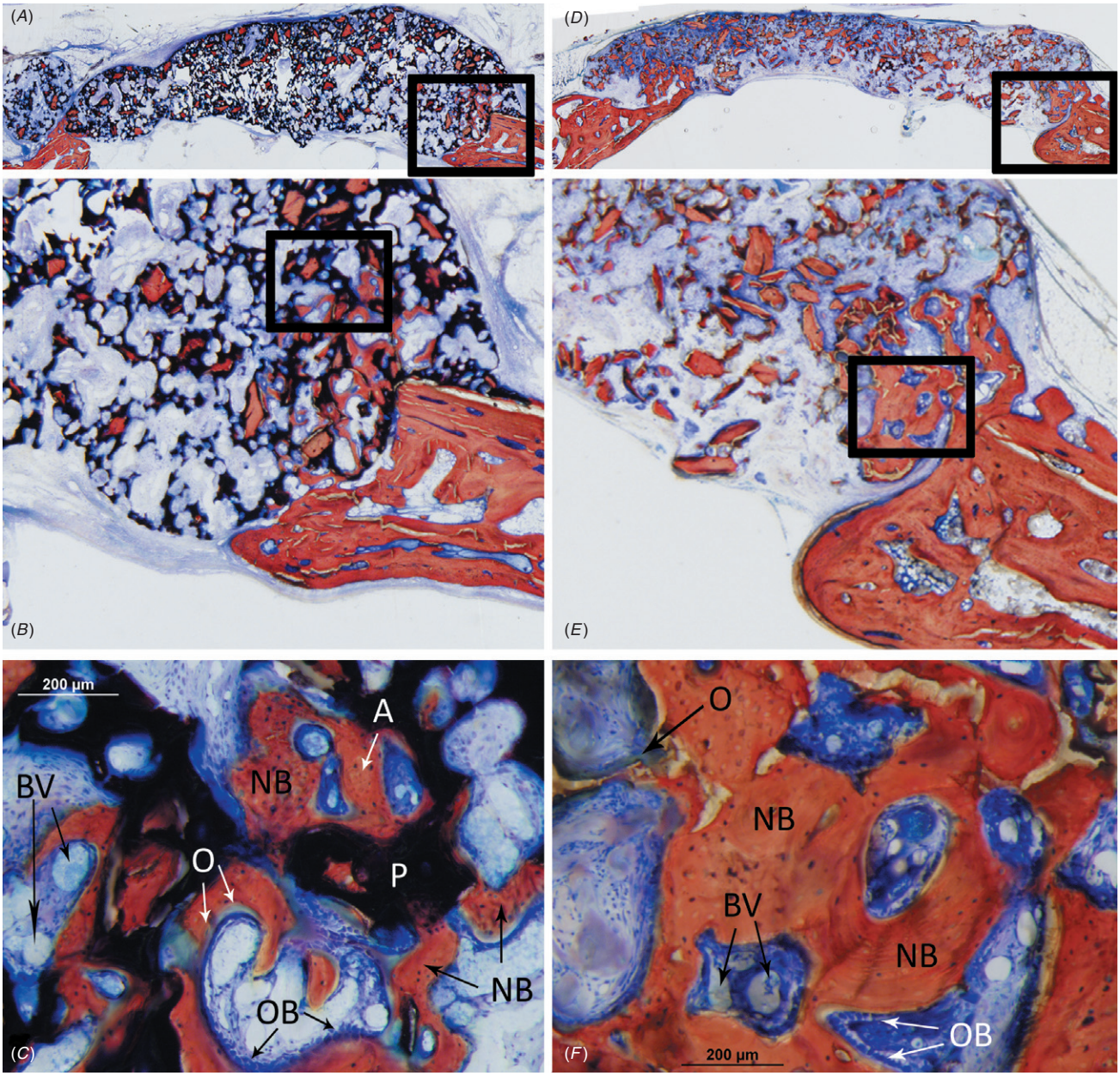

Figure 7. Representative histological sections of the biocomposites at (*A*–*C*) 6 and (*D*–*F*) 12 weeks. (*A* and *D*) Low magnification (1.6X) image of the complete defect and host bone. (*C* and *F*) High magnification (18.4X) image showing blood vessels (BV), osteoblasts (OB) and osteoid (O), new bone (NB), and residual polymer (P).

figure 8(*A*) appeared to be lower compared to the surrounding tissue, higher magnification revealed the presence of normal loose connective tissue with blood vessels surrounded by areas of newly forming bone (not shown). A higher magnification view of a region near the lower surface of the defect (figure 8(*B*)) shows both intra-membranous and endochondral new bone formation, as evidenced by the presence of cartilage (C). Areas of active remodeling characterized by osteoid (O) and osteoblasts (OB) lining the surface of the bone are evident, as well as formation of new blood vessels (BV). A higher magnification view of a region near the upper surface of the defect (figure 8(*C*)) shows residual allograft particles (A), residual polymer (black), and new bone formation (NB). Bridging of bone across the defect can also been seen in this histological section. While all rhBMP-2-treated defects showed new bone spanning the defect, calvarial defects in 5/10 animals in the BC + rhBMP-2 group had completely bridged with new bone at six weeks, which was significantly greater compared to the other treatment groups ($p < 0.0009$), in which complete bridging was not observed in any of the defects. Cells, stained light blue, migrated into pores initially present in the material due to the foaming reaction as well as those resulting from resorption of the allograft bone particles [27, 28]. Evidence of osteoclast-mediated resorption of residual allograft particles is observed in histological sections stained with TRAP (red) and hematoxylin (blue) in figure 8(*D* and *E*). TRAP-positive cells (black arrows) were observed near the surface of both residual allograft particles

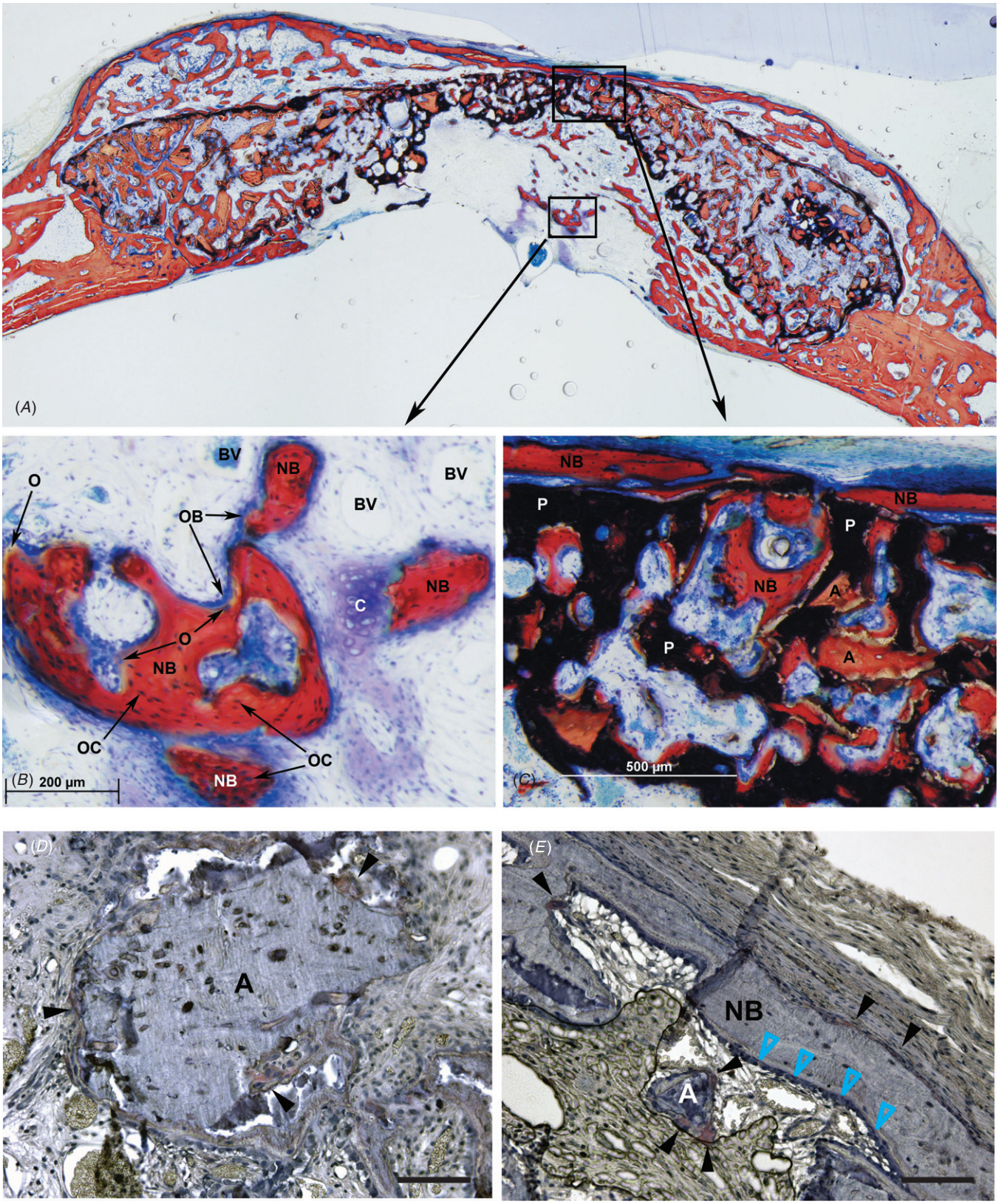

Figure 8. Representative histological sections of the biocomposites incorporating rhBMP-2 at six weeks. (*A*) Low magnification (1.6X) image of the complete defect and host bone. (*B*) High magnification (18.4X) image showing blood vessels (BV), osteoblasts (OB) and osteoid (O), osteocytes (OC), new bone (NB), and cartilage (*C*). Both intramembranous and endochondral bone formation are evident. (*C*) High magnification (10X) image of a region near the upper surface of the biocomposite showing residual polymer (P), residual allograft particles (*A*), and new bone (NB). Images (20X) of histological sections stained with TRAP (red) and hematoxylin (blue) showing (*D*) an allograft particle within the defect and (*E*) new bone bridging the defect at the upper surface. TRAP-positive cells (stained red labeled by black arrows) are evident near the surface of both residual allograft particles (Panel *D*) as well as new bone (Panel *E*). Osteoblasts (blue arrows) are also observed lining the surface of the new bone in Panel *E*. Scale bar represents 100 μm.

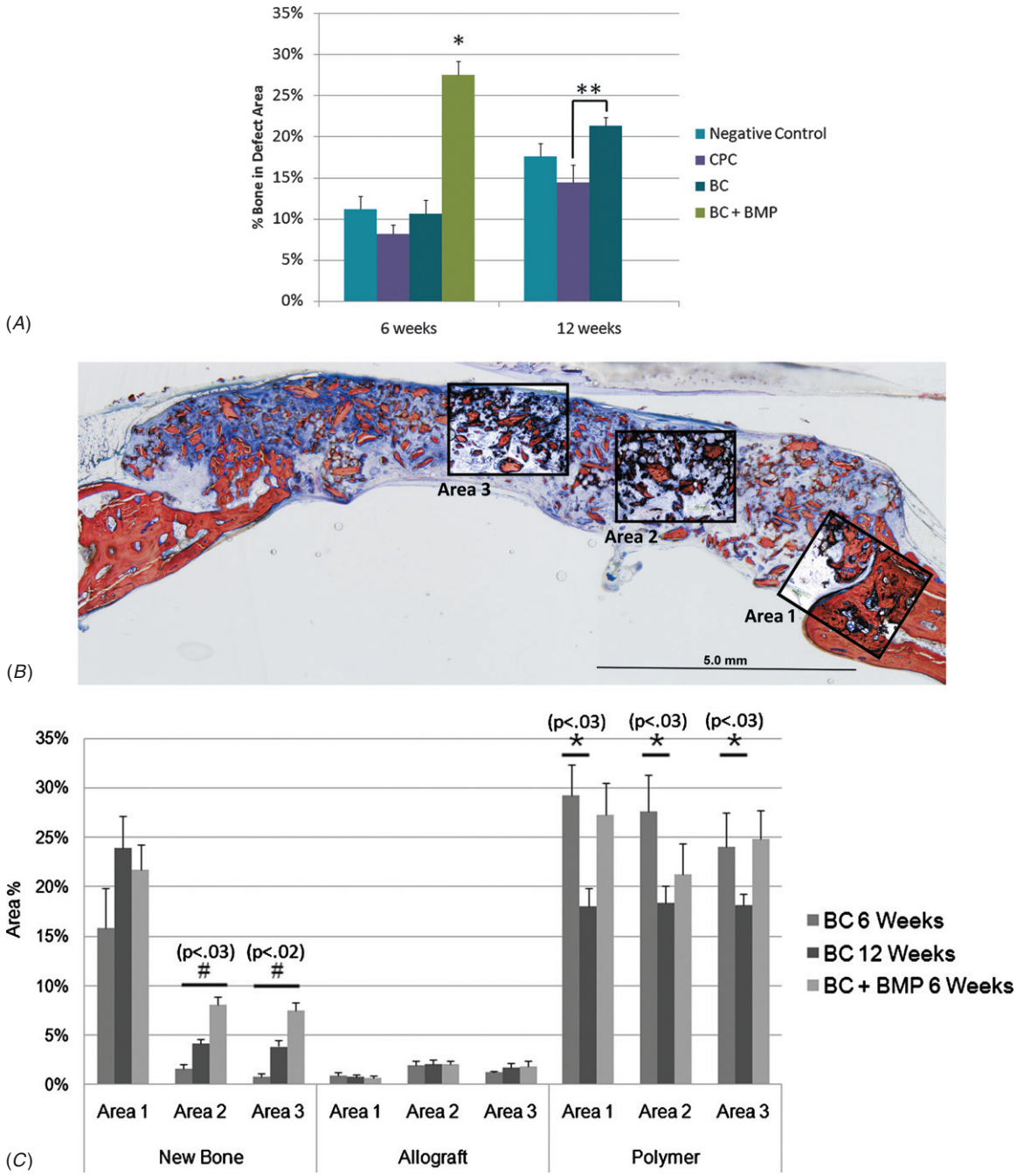

Figure 9. Histomorphometric analysis of calvarial defects. (*A*) Total bone (allograft and new bone) measured in the entire defect volume. Significantly more total bone is present in the BC + rhBMP-2 in comparison to all other treatment groups. At 12 weeks, the BC treated group has significantly more bone than the CPC treated group. (*B*) Image and schematic showing area of interest for high-magnification histomorphometric analysis required to distinguish allograft from new bone. (*C*) New bone, allograft, and polymer measured in the three representative areas progressing from the edge to the interior of the defect for the biocomposite treated groups. New bone is significantly different (#) in areas 2 ($p < 0.03$) and 3 ($p < 0.02$) for all biocomposite treatment groups. Remaining polymer is significantly less (*) for the biocomposite at 12 weeks than at 6 weeks in area 1 ($p < 0.03$).

(Panel *D, E*) as well as new bone (Panel *E*). Furthermore, osteoblasts (blue arrows) were also observed lining the surface of both the new bone and the irregularly shaped allograft particles, as shown in Panel *E*. These data suggest that the allograft component remodels by the process of creeping substitution.

Figure 9(*A*) shows the total area percent of bone measured over the entire defect area for each of the treatment groups. The bone in the biocomposites was greater than that in the Norian at both time points (though not significant at six weeks), and increased from 6 to 12 weeks. The addition of rhBMP-2 to the biocomposites resulted in significantly more bone at six weeks compared to the biocomposite at both 6 and 12 weeks without rhBMP-2. To evaluate the bone regeneration potential of the biocomposites with and without rhBMP-2 between different regions within the defect, three areas progressing from the

edge to the interior of the defect (figure 9(*B*)) were analyzed at high magnification. As shown in figure 9(*C*), new bone formation was highest in area 1 (near the host bone interface) for all three treatment groups. In the areas within the defect (areas 2 and 3) the BC at 6 weeks, the BC at 12 weeks and the BC + rhBMP-2 at 6 weeks were all significantly different from each other. The BC + rhBMP-2 group had significantly higher new bone formation in the interior areas 2 and 3. The area% of allograft was <2% for all groups in all three areas, suggesting that most of the total bone in the total defect area for the biocomposite groups (shown in figure 9(*A*)) was newly formed and not allograft. At six weeks, the area% of new bone in areas 2 and 3 was comparable to the area% of allograft. However, at 12 weeks and in the biocomposites with rhBMP-2 at six weeks, the amount of new bone in the interior areas exceeded that of residual allograft. As anticipated, the polymer decreased significantly from an initial value of 24–29 area% at week six to 18 area% at week 12 (the difference was significant only for area 1). While the residual polymer was lower at six weeks in the presence of rhBMP-2, the difference was not significant, suggesting that delivery of this relatively low amount of rhBMP-2 does not substantially affect the degradation rate of the polymer.

Discussion

Materials suitable for craniofacial repair should ideally have the ability to conform to fill complex defects, harden to temporarily protect the brain until tissue remodels, and enhance tissue regeneration through the delivery of biologics [25, 26]. In this study, we evaluated the ability of injectable polyurethane (PUR)/allograft bone biocomposites (BCs) with and without rhBMP-2 to promote bone healing in critical-size rabbit calvarial defects. The biocomposites exhibited handling properties, including working and setting times, that are comparable to those reported for CPCs [16, 35]. After injection, the biocomposites expanded to fill the defects and hardened to form a tough elastomeric solid that did not fail mechanically throughout the healing process, in contrast to the CPC that exhibited brittle fracture after cure. The mechanical integrity of the materials observed *in vivo* was consistent with their *in vitro* mechanical properties, as evidenced by the order of magnitude higher energy-to-failure of the biocomposites compared to the CPC. As early as six weeks, cells had infiltrated the biocomposites, resulting in new bone formation near the host bone/biocomposite interface, while the CPC showed minimal cellular infiltration. rhBMP-2 added to the biocomposites enhanced new bone formation, resulting in a bridge of bone covering the upper surface of the defect as well as new bone formation throughout the interior of the biocomposite.

The rheological properties of injectable and settable bone grafts must ensure ease of use in the clinic. In a previous study, we reported that the cure properties of the reactive biocomposites were comparable to the working (6–10 min) and setting (10–15 min) time requirements reported for injectable bone cements and void fillers [36, 37]. Similar to CPCs, the PUR biocomposite was shear-thinning (i.e. the viscosity decreased with increasing rate of shear stress) over a physiologically relevant range of shear rates (0.01–10 s^{-1}) [30]. Thus, the material flowed readily when extruded from the syringe. Another key parameter governing injectability is the initial (i.e. at the onset of the chemical reaction) viscosity at low shear rates prior to cure. Materials with high initial viscosity are anticipated to retain their shape after placement, while materials with low initial viscosity may continue to flow after placement and extravasate from the defect. The initial viscosity of the biocomposite at 5 s^{-1} was 170 Pa*s. In contrast, the initial viscosity of non-setting β-TCP suspensions (a model for CPCs that enables investigation of the initial rheological properties of the cement) at liquid-to-powder ratios (LPRs) of 50% and 60% ranged from 5–10 Pa*s [30]. The relatively higher initial viscosity of the biocomposites is due in part to the higher viscosity of the liquid PUR components (21 Pa*s [27] compared to 10^{-3} Pa*s for water). Low initial viscosity can also contribute to problems such as filter pressing and extravasation, which have been addressed by adding soluble polymers to the aqueous CPC mixing liquid to increase the initial viscosity [38, 39]. While addition of a 0.2% solution of Xanthan gum has been reported to increase the initial viscosity to 100 Pa*s, the added polymer also increased the yield stress (i.e. the force required to initiate flow of the material from a state of rest) from 44 Pa to 640 Pa [30]. In contrast, the biocomposites showed a yield stress of only 2.1 Pa. Taken together, the rheological data suggest that PUR biocomposites may present handling advantages compared to CPCs due to their higher initial viscosity, which minimizes filter pressing and extravasation, and relatively low yield stress, which requires a smaller force to initiate injection of the material.

Both the CPC and the biocomposite set to form a hard solid within 10 min of injection, which offers the advantage of wound closure shortly after placing the material. CPC showed extensive cracking after setting, which has been reported for CPCs in previous studies [13] and has been attributed to pulsatile forces from the dura that can drive systolic normal and tangential stresses of 54.2 kPa and 345.4 kPa, respectively [15]. In order to mitigate complications associated with Norian® CRS observed in a pediatric long-term retrospective study, use of only moderate amounts of the material has been recommended for onlay (not inlay or full calvarial thickness) applications [40]. It has also been suggested that cranioplasty materials must be sufficiently rigid to maintain space and not collapse in response to pressure from the overlying connective tissue and underlying brain tissue, but not too rigid so that they cannot conform to the contours of the defect [41]. In contrast to the CPC, the biocomposites did not reveal evidence of cracking or fragmentation either immediately after cure or at the time of explantation. The superior mechanical integrity of the biocomposite is attributed to its tougher mechanical properties, having an energy-to-failure measured under compression of 3122 ± 404 kJ m^{-3} compared to 297 ± 121 kJ m^{-3} for the CPC. While the CPC has higher modulus and yield strength than the biocomposite, it is also more brittle, characterized by a lower yield strain and energy-to-failure. Taken together, these observations suggest that the biocomposite may be more effective at providing early protection to the brain during the

early stages of the healing process due to its lower rigidity and higher toughness compared to CPC.

In addition to suitable handling and mechanical properties, rapid cellular infiltration and remodeling is another desirable attribute of injectable bone grafts. Histological sections (figure 7] showed extensive cellular infiltration for all of the biocomposite groups. As suggested by figure 8(*D–E*), cells infiltrated the biocomposites not only through migration of cells into the initial open pores, but also by migration into new pores resulting from the resorption of residual allograft particles by osteoclasts [27, 28]. These observations are in agreement with a previous study in which we reported that injectable PUR/allograft biocomposites with 40% porosity and 45 wt% allograft bone supported rapid cellular infiltration and new bone formation as early as three weeks in femoral condyle plug defects in athymic rats [27]. The vol% allograft in the biocomposite (ϕ_M) after cure is calculated from the following equation:

$$\phi_M = \frac{x_M(1-\varepsilon)}{x_M + (\rho_M/\rho_P)(1-x_M)}, \tag{3}$$

where x_M is the mass fraction allograft (or other osteoconductive matrix), ε is the porosity, $\rho_M = 2.12$ is the density of the allograft bone, and $\rho_P = 1.27$ is the density of the polymer. Thus in the present study the volume fraction of allograft in the cured biocomposite was 17.4 vol% compared to 19.7% for the athymic rat study. In the rabbit calvarial defect and athymic rat femoral plug studies, the combination of pore and allograft volumes were 61.4 and 59.7 vol%, respectively. Thus the rapid cellular infiltration of these biocomposites is consistent with the notion that cellular infiltration and remodeling proceed independent of polymer degradation when the sum of the pore and osteoconductive matrix volumes approaches 64 vol%, the random close-packing (RCP) limit for spheres [27, 28, 42].

In contrast, the CPC group showed negligible degradation and cellular infiltration, essentially acting as a barrier to bone formation over the 12 weeks. However, in a previous study we reported slow infiltration of cells into compression-molded PUR/TCP and PUR/HA composites implanted in femoral condyle defects in rats [43]. The TCP and HA granules were initially 150 μm (although the size decreased after processing due to fragmentation during compression molding), and TRAP staining revealed osteoclasts resorbing the TCP and HA particles near the bone/implant interface. Thus, dispersion of >100 μm TCP or HA particles in a polymer binder at loadings approaching the RCP limit promoted cellular infiltration and remodeling, as we have previously reported for compression-molded allograft bone particle biocomposites [28]. The negligible extent of cellular infiltration of the CPC in the present study is therefore conjectured to result from both its low specific surface area (it was not particulated) and small pore size (<1 μm) [35]. The effects of porosity, as well as the size and loading of a particulated osteoconductive matrix, on remodeling are further underscored by a recent study evaluating injectable and implantable PUR scaffolds incorporating 42 or 55 vol% porosity in a sheep femoral condyle plug defect [44]. In the absence of matrix particles, the scaffolds supported cellular infiltration and new bone formation only in open pores near the bone/implant interface. While new bone formation progressed from 6 to 24 weeks, remodeling in the interior of the material was dependent on the formation of new voids resulting from polymer degradation. Interestingly, the addition of 5 μm β-TCP particles, which have a low osteogenic potential due to their small size [45], slowed the rate of polymer degradation. The relatively low porosity (42% or 55%, which is lower than the RCP limit of 64 vol%) is conjectured to result in poor inter-connectivity, which precludes rapid cellular infiltration by migration into open pores. Thus the rate of cellular infiltration was controlled by the rate of polymer degradation, which was slow [46]. Furthermore, addition of β-TCP particles that were too small to remodel by creeping substitution (e.g., <100 μm) slowed the rate of cellular infiltration.

The PUR binder, which was initially present at 36 vol%, had degraded to 24–29 area% at week six and 18 area% at week 12. These data suggest that the polymer had degraded by 19%–33% at week six and 50% at week 12, which is in reasonable agreement with an *in vitro* study reporting 10% and 45% mass loss of the polymeric scaffold having the same composition at 6 and 12 weeks, respectively [47]. In the previous *in vitro* study, the tensile strength and modulus of the scaffolds decreased to <20% of their initial values after eight weeks of degradation time *in vitro* [47]. Considering that a substantial amount of the new bone grew appositionally to the polymer scaffold [48], excessive polymer degradation could hinder new bone formation due to the absence of a surface on which the bone could grow. Furthermore, since mechanical stability is a critical performance factor [49], especially in the calvarial defect due to the pulsatile forces emanating from the dura [15], extensive degradation of the scaffold could diminish the structural integrity of the defect in the interior regions where there was less new bone. However, despite the rapid degradation of the scaffold, significantly more bone new bone formation was observed in the center of the defect at 12 weeks compared to 6 weeks, suggesting that healing was progressing with time. While the area% polymer was less in the BC + rhBMP-2 group compared to the BC group at six weeks, the difference was not significant, which is in agreement with a previous study showing that release of rhBMP-2 did not accelerate degradation of a lysine-derived PUR scaffold at either four or eight weeks in rat femoral segmental defects [19].

Considering a previous study reporting that rabbit calvarial defects treated with rhBMP-2 delivered from an ACS carrier had completely ossified by six weeks [20], the BC + rhBMP-2 material was not evaluated at 12 weeks. When rhBMP-2 was added to the biocomposites, 75% of the defect was mineralized after six weeks. Furthermore, histological sections showed a bridge of new bone covering the upper surface of the implant as well as new bone formation throughout the defect. Bridging was complete in 50% of the rhBMP-2-treated defects. However, despite the high degree of mineralization and extensive bone bridging in the rhBMP-2-treated defects, all the defects were not completely healed at six weeks. The histological sections shown in figure 8 show progression toward healing, but additional studies are required

to demonstrate that the BC + rhBMP-2 group heals completely at later time points.

Several rhBMP-2 release strategies are under investigation as potential clinical applications [21, 50–52]. Delivery of rhBMP-2 from an absorbable collagen sponge (ACS) carrier is an FDA-approved therapeutic for treatment of posterior–lateral spine fusions, tibial fractures, and sinus and alveolar ridge augmentations. In a previous study, >90% ossification of 17 mm rabbit calvarial defects treated with the ACS carrier incorporating 430 μg mL^{-1} rhBMP-2 was reported after six weeks, compared to 30% for the empty defect negative control [20]. Similarly, >70% ossification of primate calvarial CSDs treated with the ACS carrier incorporating rhBMP-2 was observed after six months [53]. In the present study, delivery of a relatively low dose of rhBMP-2 from the biocomposites resulted in mineralization of 75 ± 3% of the defect area (as measured by radiograph analysis), which was significantly higher than the value of 15 ± 3% observed for the empty defect. While the CPC-treated defects showed comparable mineral content (82 ± 2%, figure 4(*B*)) to the rhBMP-2-treated defects, there was very little new bone (<15%) and most of the defect was filled with residual material. Histomorphometric measurements performed at high magnification revealed that the majority of the mineralized tissue in the rhBMP-2-treated defects was new bone (figure 9(*C*)). Furthermore, all rhBMP-2 treated defects showed at least partial bridging with new bone, and 50% showed complete bridging. These observations suggest that the PUR/allograft biocomposites are an efficient carrier for rhBMP-2, which is consistent with our previous study reporting that PUR scaffolds incorporating rhBMP-2 at 30% of the dose recommended for the ACS carrier supported 50% more new bone formation compared to the collagen sponge in critical-size femoral segmental defects in rats [19]. The improvement in new bone formation at sub-optimal doses was attributed to the more sustained release of rhBMP-2 from the PUR carrier, which has also been reported for a hybrid nanofiber mesh/alginate carrier [54], compared to the bolus release of rhBMP-2 from the collagen sponge. A bolus or high burst release (> 30%) is non-ideal due to the increased risk of clinical complications such as hematomas of soft tissues [51, 55]. Another limitation of the ACS carrier is that it lacks the structural integrity necessary to keep tissues from prolapsing into the site when used alone [24]. Mixed success was reported for the use of the ACS carrier without space maintenance to repair larger mandibular non-unions in five patients [23].

Extensive vascular formation in the defect was observed in the biocomposites incorporating rhBMP-2. Several *in vitro* co-culture studies have shown that osteoblasts have the capability to regulate proliferation and differentiation of endothelial cells by changing pro-angiogenic cues such as VEGF via paracrine signaling [56–58]. Furthermore, vascularization is essential for bone induction [58]. In addition to its osteoinductive and angiogenic effects, rhBMP-2 also stimulates osteoclast activity [59, 60]. Thus rhBMP-2 released from the biocomposites can accelerate the resorption of allograft bone particles [61–63] and the consequent infiltration of cells and growth of new bone in the newly formed pores. However, the low dose of rhBMP-2 used in this study did not accelerate allograft resorption.

Conclusion

Reactive PUR/allograft bone biocomposites exhibit favorable injectability, characterized by a relatively low yield stress to initiate flow of the material and a relatively high initial viscosity to minimize the adverse phenomena of extravasation and filter pressing. After injection, the biocomposites cure within 10–12 min to form a tough, elastomeric solid that maintains mechanical integrity during the healing process, in contrast to the CPC which undergoes brittle fracture. When injected into a rabbit calvarial CSD, the biocomposites supported ingrowth of new bone near the host bone/biocomposite interface, and the addition of a low dose of rhBMP-2 (80 μg mL^{-1}) enhanced new bone formation throughout the volume of the defect. Thus, injectable reactive PUR/allograft biocomposites are a promising approach for healing calvarial defects by providing both mechanical stability as well as local delivery of rhBMP-2.

Acknowledgments

The opinions or assertions contained herein are the private views of the authors and are not to be construed as official or as reflecting the views of the Department of the Army or the Department of Defense. This work was supported by the Armed Forces Institute of Regenerative Medicine (AFIRM), the U.S. Army Institute of Surgical Research, and the National Science Foundation through a CAREER award to SAG (DMR0847711). The Armed Forces Institute of Regenerative Medicine (AFIRM) is managed and funded through the U.S. Army Medical Research and Materiel Command, with additional funding from the U.S. Navy, Office of Naval Research; the U.S. Air Force, Office of the Surgeon General; the National Institutes of Health; the Veterans Administration; and local public and private matching funding. Rutgers-Cleveland Clinic Consortium of AFIRM is funded by Department of Defense, USA Medical Research Acquisition (ACQ) Activity contract no W81XWH-08-2-0034.

References

[1] Ueeck B A 2007 Penetrating injuries to the face: delayed versus primary treatment—considerations for delayed treatment *J. Oral Maxillofac. Surg.* **65** 1209–14

[2] Shermak M A, Wong L, Inoue N and Nicol T 2000 Reconstruction of complex cranial wounds with demineralized bone matrix and bilayer artificial skin *J. Craniofac. Surg.* **11** 224–31

[3] Lemperle S M, Calhoun C J, Curran R W and Holmes R E 1998 Bony healing of large cranial and mandibular defects protected from soft-tissue interposition: a comparative study of spontaneous bone regeneration, osteoconduction, and cancellous autografting in dogs *Plast. Reconstr. Surg.* **101** 660–72

[4] Khan Y, Yaszemski M J, Mikos A G and Laurencin C T 2008 Tissue engineering of bone: material and matrix considerations *J. Bone Joint Surg. Am.* **90** (Suppl. 1) 36–42

[5] Chim H and Gosain A K 2009 Biomaterials in craniofacial surgery experimental studies and clinical application *J. Craniofac. Surg.* **20** 29–33

[6] Tessier P 1982 Autogenous bone grafts taken from the calvarium for facial and cranial applications *Clin. Plast. Surg.* **9** 531–8

[7] Wan D C *et al* 2006 Differential gene expression between juvenile and adult dura mater: a window into what genes play a role in the regeneration of membranous bone *Plast. Reconstr. Surg.* **118** 851–61

[8] Smith D M, Cooper G M, Mooney M P, Marra K G and Losee J E 2008 Bone morphogenetic protein 2 therapy for craniofacial surgery *J. Craniofac. Surg.* **19** 1244–59

[9] Lew T A, Walker J A, Wenke J C, Blackbourne L H and Hale R G 2009 Characterization of craniomaxillofacial battle injuries sustained by United States service members in the current conflicts of Iraq and Afghanistan *J. Oral Maxillofac. Surg.* **68** 3–7

[10] Kauvar D S, Wolf S E, Wade C E, Cancio L C, Renz E M and Holcomb J B 2006 Burns sustained in combat explosions in operations Iraqi and enduring freedom (OIF/OEF explosion burns) *Burns* **32** 853–7

[11] Schmitz J P, Hollinger J O and Milam S B 1999 Reconstruction of bone using calcium phosphate bone cements: a critical review *J. Oral Maxillofac. Surg.* **57** 1122–6

[12] Elshahat A, Shermak M A, Inoue N, Chao E Y and Manson P 2004 The use of Novabone and Norian in cranioplasty: a comparative study *J. Craniofac. Surg.* **15** 483–9

[13] Moghadam H G, Sandor G K, Holmes H H and Clokie C M 2004 Histomorphometric evaluation of bone regeneration using allogeneic and alloplastic bone substitutes *J. Oral Maxillofac. Surg.* **62** 202–13

[14] Clokie C M, Moghadam H, Jackson M T and Sandor G K 2002 Closure of critical sized defects with allogenic and alloplastic bone substitutes *J. Craniofac. Surg.* **13** 111–21

[15] Goldberg C S, Antonyshyn O, Midha R and Fialkov JA 2005 Measuring pulsatile forces on the human cranium *J. Craniofac. Surg.* **16** 134–9

[16] Bohner M 2011 Designing ceramics for injectable bone graft substitutes *Injectable Biomaterials: Science and Applications* ed BL Vernon (Philadelphia, PA: Woodhead Publishing)

[17] Spector J, Luchs J, Mehera B, Greenwald J, Smith L and Longaker M 2001 Expression of bone morphogenetic proteins during membranous bone healing *Plast. Reconstr. Surg.* **107** 124–34

[18] Boerckel J D *et al* 2011 Effects of protein dose and delivery system on BMP-mediated bone regeneration *Biomaterials* **32** 5241–51

[19] Brown K V, Li B, Guda T, Perrien D S, Guelcher S A and Wenke J C 2011 Improving bone formation in a rat femur segmental defect by controlling bone morphogenetic protein-2 release *Tissue Eng.* A **17** 1735–46

[20] Smith D M, Afifi A M, Cooper G M, Mooney M P, Marra K G and Losee J E 2008 BMP-2-based repair of large-scale calvarial defects in an experimental model: regenerative surgery in cranioplasty *J. Craniofac. Surg.* **19** 1315–22

[21] Haidar Z S, Hamdy R C and Tabrizian M 2009 Delivery of recombinant bone morphogenetic proteins for bone regeneration and repair: part A. Current challenges in BMP delivery *Biotechnol. Lett.* **31** 1817–24

[22] McKay W F, Peckham S M and Badura J M 2007 A comprehensive clinical review of recombinant human bone morphogenetic protein-2 (INFUSE Bone Graft) *Int. Orthop.* **31** 729–34

[23] Carter T G, Brar P S, Tolas A and Beirne O R 2008 Off-Label use of recombinant human bone morphogenetic protein-2 (rhBMP-2) for reconstruction of mandibular bone defects in humans *J. Oral Maxillofac. Surg.* **66** 1417–25

[24] Herford A S and Boyne P J 2008 Reconstruction of mandibular continuity defects with bone morphogenetic protein-2 (rhBMP-2) *J. Oral Maxillofac. Surg.* **66** 616–24

[25] Panetta N J, Gupta D M and Longaker M T 2009 Bone tissue engineering scaffolds of today and tomorrow *J. Craniofac. Surg.* **20** 1531–2

[26] Hollister S J *et al* 2005 Engineering craniofacial scaffolds *Orthod. Craniofac. Res.* **8** 162–73

[27] Dumas J E, Zienkiewicz K, Tanner S A, Prieto E M, Bhattacharyya S and Guelcher S 2010 Synthesis and characterization of an injectable allograft bone/polymer composite bone void filler with tunable mechanical properties *Tissue Eng.* A **16** 2505–18

[28] Dumas J E *et al* 2010 Synthesis of allograft bone/polymer composites and evaluation of remodeling in a rabbit femoral condyle model *Acta Biomater.* **6** 2394–406

[29] Li J Q and Salovey R 2004 Model filled polymers: the effect of particle size on the rheology of filled poly(methyl methacrylate) composites *Polym. Eng. Sci.* **44** 452–62

[30] Baroud G, Cayer E and Bohner M 2005 Rheological characterization of concentrated aqueous beta-tricalcium phosphate suspensions: the effect of liquid-to-powder ratio, milling time, and additives *Acta Biomater.* **1** 357–63

[31] Luvizuto E R *et al* 2011 The effect of BMP-2 on the osteoconductive properties of beta-tricalcium phosphate in rat calvaria defects *Biomaterials* **32** 3855–61

[32] An Y H and Friedman R J 1999 Animal models of bone defect repair *Animals Models in Orthopaedic Research* ed Y H An and R J Friedman (Boca Raton, FL: CRC Press)

[33] Otsu N 1978 A threshold selection method for gray level histogram *IEEE Trans. Syst. Man Cybern.* **SMC-9** 62–66

[34] Elsalanty M E *et al* 2008 Recombinant human BMP-2 enhances the effects of materials used for reconstruction of large cranial defects *J. Oral Maxillofac. Surg.* **66** 277–85

[35] Bohner M 2000 Calcium orthophosphates in medicine: from ceramics to calcium phosphate cements *Injury* **31** (Suppl. 4) S-D37–47

[36] Lewis G 2007 Percutaneous vertebroplasty and kyphoplasty for the stand-alone augmentation of osteoporosis-induced vertebral compression fractures: present status and future directions *J. Biomed. Mater. Res., Appl. Biomater.* **81B** 371–86

[37] Clarkin O M, Boyd D, Madigan S and Towler M R 2009 Comparison of an experimental bone cement with a commercial control, Hydroset™ *J. Mater. Sci., Mater. Med.* **20** 1563–70

[38] Bohner M and Baroud G 2005 Injectability of calcium phosphate pastes *Biomaterials* **26** 1553–63

[39] Cherng A, Takagi S and Chow L C 1997 Effects of hydroxypropyl methylcellulose and other gelling agents on the handling properties of calcium phosphate cement *J. Biomed. Mater. Res.* **35** 273–7

[40] Gilardino M S, Cabiling D S and Bartlett S P 2009 Long-term follow-up experience with carbonated calcium phosphate cement (Norian) for cranioplasty in children and adults *Plast. Reconstr. Surg.* **123** 983–94

[41] Aaboe M, Pinholt E M, Schou S and Hjorting-Hansen E 1998 Incomplete bone regeneration of rabbit calvarial defects using different membranes *Clin. Oral Implants Res.* **9** 313–20

[42] Torquato S, Truskett T M and Debenedetti P G 2000 Is random close packing of spheres well defined ? *Phys. Rev. Lett.* **84** 2064–7

[43] Yoshii T, Dumas J E, Okawa A, Spengler D M and Guelcher S A 2012 Synthesis, characterization of calcium phosphates/polyurethane composites for

weight-bearing implants *J. Biomed. Mater. Res., Appl. Biomater.* B **100** 32–40
[44] Adhikari R *et al* 2008 Biodegradable injectable polyurethanes: synthesis and evaluation for orthopaedic applications *Biomaterials* **29** 3762–70
[45] Malinin T I, Carpenter E M and Temple H T 2007 Particulate bone allograft incorporation in regeneration of osseous defects; importance of particle sizes *Open Orthop. J.* **1** 19–24
[46] Hasegawa S *et al* 2006 A 5–7 year *in vivo* study of high-strength hydroxyapatite/poly(L-lactide) composite rods for the internal fixation of bone fractures *Biomaterials* **27** 1327–32
[47] Hafeman A E *et al* 2011 Characterization of the degradation mechanisms of lysine-derived aliphatic poly(ester urethane) scaffolds *Biomaterials* **32** 419–29
[48] Li B, Yoshii T, Hafeman A E, Nyman J S, Wenke J C and Guelcher S A 2009 The effects of rhBMP-2 released from biodegradable polyurethane/microsphere composite scaffolds on new bone formation in rat femora *Biomaterials* **30** 6768–79
[49] Donath K, Laass M and Gunzl H J 1992 The histopathology of different foreign-body reactions in oral soft tissue and bone tissue *Virchows Arch. A, Pathol. Anat. Histopathol.* **420** 131–7
[50] Takaoka K, Koezuka M and Nakahara H 1991 Telopeptide-depleted bovine skin collagen as a carrier for bone morphogenetic protein *J. Orthop. Res.* **9** 902–7
[51] Haidar Z S, Hamdy R C and Tabrizian M 2009 Delivery of recombinant bone morphogenetic proteins for bone regeneration and repair: part B. Delivery systems for BMPs in orthopaedic and craniofacial tissue engineering *Biotechnol. Lett.* **31** 1825–35
[52] Miyazaki M *et al* 2009 A porcine collagen-derived matrix as a carrier for recombinant human bone morphogenetic protein-2 enhances spinal fusion in rats *Spine J.* **9** 22–30
[53] Sheehan J P, Sheehan J M, Seeherman H, Quigg M and Helm G A 2003 The safety and utility of recombinant human bone morphogenetic protein-2 for cranial procedures in a nonhuman primate model *J. Neurosurg.* **98** 125–30
[54] Kolambkar Y M *et al* 2011 An alginate-based hybrid system for growth factor delivery in the functional repair of large bone defects *Biomaterials* **32** 65–74
[55] Geiger M, Li R H and Friess W 2003 Collagen sponges for bone regeneration with rhBMP-2 *Adv. Drug Deliv. Rev.* **55** 1613–29
[56] Santos M I, Unger R E, Sousa R A, Reis R L and Kirkpatrick C J 2009 Crosstalk between osteoblasts and endothelial cells co-cultured on a polycaprolactone-starch scaffold and the *in vitro* development of vascularization *Biomaterials* **30** 4407–15
[57] Unger R E *et al* 2007 Tissue-like self-assembly in cocultures of endothelial cells and osteoblasts and the formation of microcapillary-like structures on three-dimensional porous biomaterials *Biomaterials* **28** 3965–76
[58] Szpalski M and Gunzburg R 2005 Recombinant human bone morphogenetic protein-2: a novel osteoinductive alternative to autogenous bone graft? *Acta Orthop. Belg.* **71** 133–48
[59] Jensen E D *et al* 2010 Bone morphogenic protein 2 directly enhances differentiation of murine osteoclast precursors *J. Cell Biochem.* **109** 672–82
[60] Okamoto M, Murai J, Yoshikawa H and Tsumaki N 2006 Bone morphogenetic proteins in bone stimulate osteoclasts and osteoblasts during bone development *J. Bone Miner Res.* **21** 1022–33
[61] Belfrage O, Flivik G, Sundberg M, Kesteris U and Tagil M 2011 Local treatment of cancellous bone grafts with BMP-7 and zoledronate increases both the bone formation rate and bone density *Acta Orthop.* **82** 228–33
[62] Schwartz Z *et al* 1998 Addition of human recombinant bone morphogenetic protein-2 to inactive commercial human demineralized freeze-dried bone allograft makes an effective composite bone inductive implant material *J. Periodontol.* **69** 1337–45
[63] McGee M A *et al* 2004 The use of OP-1 in femoral impaction grafting in a sheep model *J. Orthop. Res.* **22** 1008–15